Received: 18 October 2023 | Revised: 25 November 2023 | Accepted: 27 December 2023

DOI: 10.1002/prot.26663

RESEARCH ARTICLE

PROTEINS WILEY

Mechanistic study of the transmission pattern of the SARS-CoV-2 omicron variant

Ke An[1,2,3] | Xianzhi Yang[4] | Mengqi Luo[5] | Junfang Yan[1,2] | Peiyi Xu[1,2] | Honghui Zhang[1,2] | Yuqing Li[6] | Song Wu[6] | Arieh Warshel[7] | Chen Bai[1,2,3]

[1]School of Life and Health Sciences, School of Medicine, The Chinese University of Hong Kong, Shenzhen, Guangdong, China

[2]Warshel Institute for Computational Biology, Shenzhen, China

[3]Chenzhu (MoMeD) Biotechnology Co., Ltd, Hangzhou, Zhejiang, China

[4]Institute of Urology, The Third Affiliated Hospital of Shenzhen University (Luohu Hospital Group), Shenzhen, China

[5]College of Management, Shenzhen University, Shenzhen, China

[6]Department of Urology, South China Hospital of Shenzhen University, Shenzhen, China

[7]Department of Chemistry, University of Southern California, Los Angeles, California, USA

Correspondence
Song Wu, Department of Urology, South China Hospital of Shenzhen University, Shenzhen 518116, China.
Email: wusong@szu.edu.cn

Arieh Warshel, Department of Chemistry, University of Southern California, Los Angeles, CA 90089-1062, USA.
Email: warshel@usc.edu

Chen Bai, School of Life and Health Sciences, School of Medicine, The Chinese University of Hong Kong, Shenzhen, Guangdong 518172, China.
Email: baichen@cuhk.edu.cn

Funding information
2021 Basic Research General Project of Shenzhen, China, Grant/Award Number: 20210316202830001; Shenzhen Science Technology and Innovation Commission of Shenzhen Municipality, Grant/Award Number: RCJC20200714114557005; National Natural Science Foundation of China, Grant/Award Number: 61931024; National Science Foundation, Grant/Award Number: MCB 2142727; National Institutes of Health, Grant/Award Number: GM122472; The Warshel Institute for computational Biology Funding

Abstract

The omicron variant of severe acute respiratory syndrome coronavirus 2 (SARS-CoV-2) characterized by 30 mutations in its spike protein, has rapidly spread worldwide since November 2021, significantly exacerbating the ongoing COVID-19 pandemic. In order to investigate the relationship between these mutations and the variant's high transmissibility, we conducted a systematic analysis of the mutational effect on spike–angiotensin-converting enzyme-2 (ACE2) interactions and explored the structural/energy correlation of key mutations, utilizing a reliable coarse-grained model. Our study extended beyond the receptor-binding domain (RBD) of spike trimer through comprehensive modeling of the full-length spike trimer rather than just the RBD. Our free-energy calculation revealed that the enhanced binding affinity between the spike protein and the ACE2 receptor is correlated with the increased structural stability of the isolated spike protein, thus explaining the omicron variant's heightened transmissibility. The conclusion was supported by our experimental analyses involving the expression and purification of the full-length spike trimer. Furthermore, the energy decomposition analysis established those electrostatic interactions make major contributions to this effect. We categorized the mutations into four groups and established an analytical framework that can be employed in studying future mutations. Additionally, our calculations rationalized the reduced affinity of the omicron variant towards most available therapeutic neutralizing antibodies, when compared with the wild type. By providing concrete experimental data and offering a solid explanation, this study contributes to a

Ke An, Xianzhi Zhang, and Mengqi Luo contributed equally to this work.

better understanding of the relationship between theories and observations and lays the foundation for future investigations.

KEYWORDS
computational biology, omicron, SARS-CoV-2, spike protein

1 | INTRODUCTION

The severe acute respiratory syndrome coronavirus 2 (SARS-CoV-2) virus caused the global COVID-19 pandemic and killed 7 million people in past several years. The virus has been continuously evolved and gave rise to many variants with enhanced virulence, which exacerbated the epidemic and were defined as VOC (variant of concern),[1] such as alpha (B.1.1.7), beta (B.1.351), gamma (P.1), delta (B.1.617.2), and omicron (B.1.1.529). Numerous experimental studies have already explored the connections between mutations and their impact on transmissibility, infectivity, and evasion of immune responses. For instance, the alpha variant, with an N501Y substitution in its S protein, demonstrates higher transmissibility compared with the original SARS-CoV-2.[2] The beta and gamma variants, which carry the E484K substitution, show strong resistance to neutralizing antibodies produced by vaccination and natural SARS-CoV-2 infection.[3–6] Mutations in the furin cleavage site region (P681H, H655Y, N679K) reduce S1/S2 cleavage, fusogenicity, and syncytia formation associated with pathogenesis.[7] Research by Escalera et al.[8] indicates that the 655Y spike polymorphism, present in the gamma and omicron variants, plays a crucial role in SARS-CoV-2 infection and transmission.

The omicron variant (B.1.1.529) emerged in 11th 2020 with three to six times transmission speed than the wild type and spread to five continents in 1 month.[9,10] Since November 2021, omicron replaced other VOCs as the dominant strain, brought another blow to the pandemic response and added more uncertainties.[9–13] This variant showed fast spreading speed and resistance to many neutralizing antibodies[14–16] but exhibited lower risk of severe illness or fatality than other VOCs.[17] In order to understand the reasons behind the spread of the COVID-19 pandemic, it is important to explore the origin of the high omicron's transmissibility to provide clues to possible transmissible variants in the future.[18]

The omicron variant carries the largest number of mutations (a total of 60 mutations) compared with previous VOCs, including several well-known mutations such as E484K, N501Y, and N478K. Some mutations appeared for the first time. More than half of mutations happens on the spike protein, the requisite functional factor for virus entry.[19] The spike protein interacts with the human host cell surface receptor angiotensin-converting enzyme-2 (ACE2) through its receptor-binding domain (RBD).[20] Mutations of this protein result in 30 amino acid substitutions with 15 located on RBD. According to the relevant crystal structure data, despite so many mutations, the RBD conformation of omicron does not change significantly.[21] The binding affinity of spike protein and ACE2 correlates with the spreading speed,[22] the infectivity,[23] and the population of the variants.[24] Therefore, the effect of mutations on RBD may be reflected in the RBD-ACE2 binding free energy, but it is not clear what is the relationship between the spreading efficiency and the binding affinity of the omicron variant and the receptor.

In addition to the RBD of spike, numerous mutations outside of this domain have been found to impact the transmissibility of the virus. These mutations not only influence the interaction between the spike protein and ACE2 receptor, but also affect the overall structural stability, the cleavage efficiency, and the immunogenicity of the spike trimer. One notable example is the D614G mutation located in the SD1/2 region, which has been shown to significantly enhance the fusogenicity and infectivity of the virus in SARS-CoV-2 VoCs such as alpha, beta, and omicron.[25] This enhancement may be attributed to an increased spike-ACE2 binding affinity potentially resulting from local spatial flexibility induced by the D614G mutation.[26] However, it is worth noting that many current studies on spike protein mutations have primarily focused on the RBD region.[27,28] Thus, there is a pressing need for systematic investigations into the full-length spike trimer of the SARS-CoV-2 virus.

Yin et al.,[21] McCallum et al.,[29] ZHANG et al.,[30] and Hong et al.[31] solved structures of the spike protein of the omicron variant by cryo-electron microscopy (Cryo-EM). They all agreed on the proposal that the omicron variant has a stronger binding affinity to ACE2, and analyzed the structural basis for the binding enhancement. However, these studies have not provided a way to obtain the mutational-induced changes in the binding free energies. At any rate, it is essential to elucidate the mutational effects on the omicron binding.

Some approaches have been reported for investigating the effects of different mutations on the virus, such as long molecular dynamics simulation,[32–34] machine learning,[35–37] engineered ACE2 receptor design,[38–42] and structural analysis,[43–48] and so forth. Most studies analyzed the structural differences of the mutants, but did not relate such structural changes to binding energies. It is also important to mention that some experimental studies detected the conformational dynamics[49] and the mutational effects on the conformational stability[50] of the SARS-CoV-2 spike protein. However, these studies still have not provided a way to obtain reliable mutational-induced changes in binding free energies that can be used for fast screening of key mutational sites.

In previous works, we investigated the binding patterns and mutational effects of the SARS-CoV-2 spike protein in an energic view. Our early work[51] explored the structure/energy basis of the binding energy of spike/ACE2 using our coarse-grained (CG) model[52–54] and Monte Carlo proton transfer (MCPT) method,[52] this study predicted that specific mutations at Q493, Q498, and N501 of spike protein might lead to stronger binding of ACE2, ahead of the appearance of the alpha variant.[51] Using the same methods, we

systemically investigate the structure/energy basis of the alpha, beta, and delta variants.[55] The results explained the mutational effect of Q493 and Q498 predicted in[51] and the results were supported by experiments.[55] Subsequently, these two mutations occurred in the omicron variant. These works provided a proof of principle and confirmed the validity of our methods.

This study presents a comprehensive evaluation of energy calculations and structural analyses pertaining to the omicron variant's single and combined mutational sites. To overcome the computational challenges, we employed a CG model,[52–54] which replaces the all-atom (AA) model, enabling us to effectively model the full-length spike trimer. The CG models of the mutated proteins were constructed based on the cryo-EM structure of the wild-type spike/ACE2 complex. Our energy calculation confirmed a stronger binding affinity between the spike protein of the omicron variant and the ACE2 receptor when compared with the delta variant. Notably, the structural stability of the spike protein in the omicron variant exhibited significant enhancement, distinguishing it from other VOCs. These computational trends were further validated though an experimental study that involved the expression and purification of the full-length spike trimer. By analyzing the energy contribution, we identified key residues that play crucial roles in the enhanced binding affinity and structural stability. Furthermore, we categorized the mutations into four groups, establishing an analytical framework to guide future studies. In addition, we predicted potential mutation sites that have yet to be explored in existing studies. Remarkably, our calculations revealed decreased binding affinities between the spike protein of the omicron variant to several SARS-CoV-2 therapeutic antibodies, when compared with the wild type. This finding suggests the possibility that reduced antibody binding may contribute to the high transmission of the omicron variant, posing challenges to current vaccination and treatment strategies. Through providing an energy-based explanation for the heightened transmissibility of the omicron variant and enhancing our understanding of the underlying mechanisms driving these mutations, our research stands as a pioneering work. It not only offers valuable experimental data but also provides a solid theoretical foundation in elucidating the relationship between theoretical predictions and observed phenomena. Ultimately, this collection of empirical evidence and corresponding theoretical insights will serve as a guiding force for future investigations.

2 | RESULTS

2.1 | The omicron variant has stronger binding affinity than the delta variant

In order to determine whether omicron variant has a stronger binding affinity with ACE2 than the delta variant, we calculated the relative binding energy change ($\Delta\Delta G$). This $\Delta\Delta G$ is the difference in the binding free energy to ACE2, between the mutated ($\Delta G_{\text{binding}_{\text{mutant}}}$) and the wild-type ($\Delta G_{\text{binding}_{\text{WT}}}$) spike protein ($\Delta\Delta G = \Delta G_{\text{binding}_{\text{mutant}}} - \Delta G_{\text{binding}_{\text{WT}}}$). A larger negative $\Delta\Delta G$ suggests a stronger binding affinity. Previous studies have found that the delta variant showed an enhancement of the binding affinity compared with wild type,[55] thus here we also calculated the $\Delta\Delta G$ of the delta variant as control. The calculation gave for omicron a $\Delta\Delta G$ of −16.4 kcal/mol whereas the corresponding value for delta is −10.5 kcal/mol. This suggests omicron has a stronger binding affinity than delta (Figure 1 and Table S1). This may explain the fact that the omicron variant has six times higher transmissibility than delta.[9,10]

Next, we investigated the effect of specific single mutations on the stronger affinity. We calculated $\Delta\Delta G$ of each individual mutation of the omicron variant's spike protein. Of the 33 mutations (including 3 deletions and 30 amino acid substitutions), 7 located in the N-terminal domain (NTD), 15 were in the RBD, and 11 were in the regions in which other VOCs show few mutations, including the SD1/2, HR1, and other unnamed regions (Figure 1).[29] Many important antigens distributed in spike's NTD,[56] which may alter the antigenic surface of omicron and account for the loss of binding and neutralization by antibodies.[30,56] This is also consistent with the observation that the omicron variant can infect people who have been immune to other variants.[9,10,14,57]

Mutations of the RBD show significant contribution to spike's enhanced binding affinity. Figure 1 shows the binding free energy change following individual or combined mutational sites of omicron variant. Most of these mutations exhibit a favorable trend for binding to ACE2 with a negative $\Delta\Delta G$, except for H655Y (0.65 kcal/mol) and K417N (0.98 kcal/mol). H655Y, who locates in the SD1/2 region and also present in the gamma variant, does not significantly change the complex structure, but change the interaction between H655 and F643 and result in destabilization of the protein structure.[30] K417N is also found in other variants and locates at the RBD/ACE2 interface. This mutation reduces the ACE2 affinity by destroying the ionic interactions with ACE2.[29,43,44] Most mutations in RBD show enhanced binding affinity than in other regions (Figure 1 and Table S1). T478K, which also occurred in delta, demonstrates the largest binding affinity enhancement with $\Delta\Delta G = -4.96$ kcal/mol. Other mutations, which first occurred in the omicron variant, such as N440K (−3.93 kcal/mol), Q493R (−3.01 kcal/mol), Q498R (−1.42 kcal/mol), and Y505H (−2.05 kcal/mol), also show significant increase in binding.

These individual mutations show a synergistic trend in affecting the spike protein. When they combined, the $\Delta\Delta G$ values of the omicron variant is not simply a linear combination of each individual contribution, but higher than the sum (−16.48 vs. −30.87 kcal/mol). However, omicron's $\Delta\Delta G$ is much more negative than that of any individual mutation (Figure 1). These results imply the epistasis of these mutations.[55] Considering these, it is worth to explore the mechanism of the structural/energetic basis of the stronger binding effect of omicron variant's mutations at a molecular level.

2.2 | Both structural stability and binding affinity of the omicron variant's spike were enhanced

By decomposing $\Delta\Delta G$, we found that the omicron spike/ACE2 complex and the isolated omicron spike protein are stabilized with $\Delta G_1 = -30.34$ and $\Delta G_2 = 13.86$ kcal/mol, respectively (Table S2, see Section 4, ΔG_1, ΔG_2 are defined in Equation 3). The energy amplitude of the complex stabilization is much larger than the isolated spike protein stabilization. The extra portion is contributed by the enhanced spike/ACE2 binding affinity.

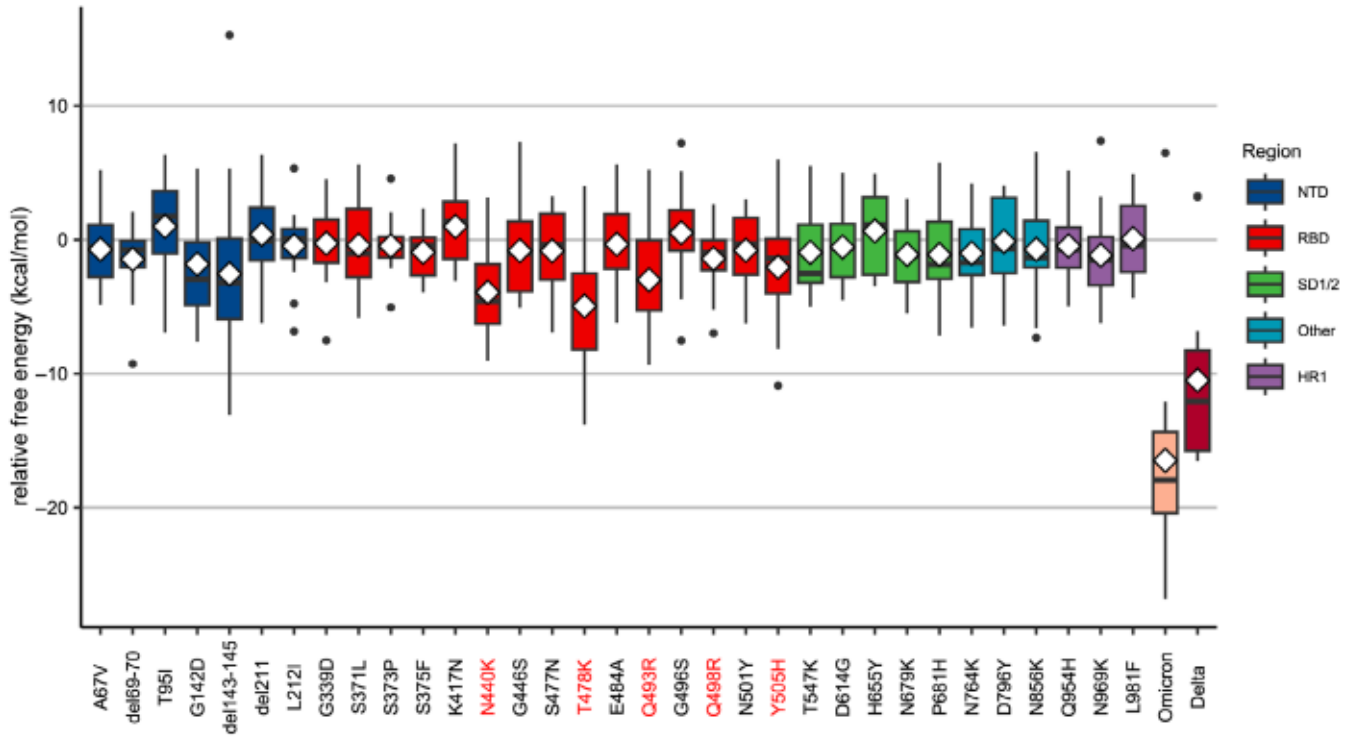

FIGURE 1 The binding free energy change of each mutation of omicron or combinations of all sites of the omicron and delta variant. The square and line represent the statistics of 15 data points (see Section 4); the diamond designates the average value of each square line (Table S1); the points designate the outliers of the data; the color designates in which region the mutated site is located: N-terminal Domain (blue), Receptor Binding Domain (red), Subdomain 1/2 (green), other unnamed regions (cyan), Heptad Repeat 1 (purple). The text under the x-axis represents the name of mutations or variants, where the red text indicates the mutations with the largest magnitude of ΔΔG.

Further, we decomposed ΔG_1 and ΔG_2 into individual terms (Table S2) and found that the electrostatic term (G_e) is mainly dominated for free-energy change. This finding highlights the dominant role of electrostatic interactions in determining the free energy profile of biophysical systems.[53,58–62] As we have emphasized before, in order to analyze the effect of electrostatic interaction change around a mutated site, we should take into account the overall electrostatic field change and not just discuss interactions between the mutated site and its nearby residues.[55] The hydrophobic term also plays a role in determining the stabilization of the system, but its contribution is about 1/3 of that of electrostatic term (Table S2).

We also calculated the free energy of other variants. The results show that other variants' spike proteins are led to destabilization (beta: $\Delta G_2 = -3.53$; gamma: $\Delta G_2 = -3.43$; delta: $\Delta G_2 = -8.8$), except for the alpha variant ($\Delta G_2 = 0.6$). This indicates the substantial enhancement of spike's structural stability may be one of the characteristics that distinguishes omicron from other variants.

2.3 | Analyzing individual electrostatic contributions

To identify key residues contributing to binding affinity and structural stability, we evaluated the electrostatic energy change (ΔG_e) between each charged residue of omicron and wild-type spike/ACE2

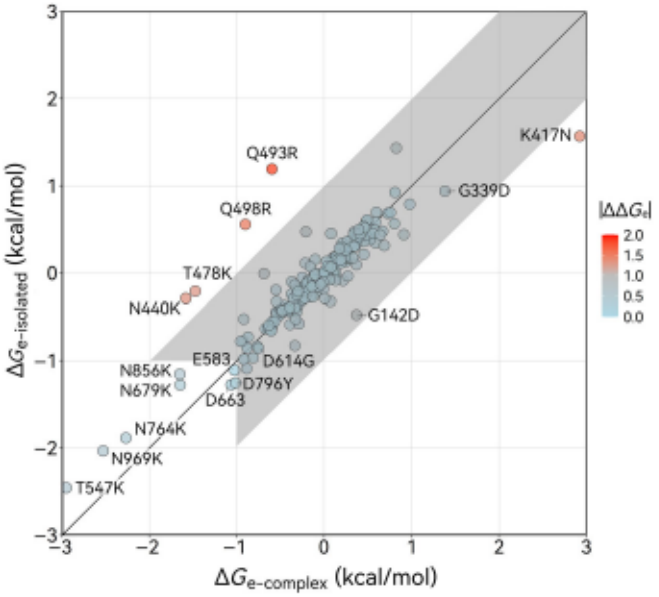

FIGURE 2 The relative magnitude of electrostatic free energy contribution $\Delta G_e = G_{omicron} - G_{wildtype}$ of each charged residue in complex or in isolated spike protein. The color of points designates the difference of energy contribution ($|\Delta\Delta G_e| = |\Delta G_{e\text{-complex}} - \Delta G_{e\text{-spike}}|$). The shaded region designates all points that do not meet the two criteria of key residues defined in the main text. The key residues identified are marked by texts. $R^2 = 0.7732$.

complexes ($\Delta G_{e\text{-complex}}$), as well as the ΔG_e contribution for the interactions between the isolated omicron and wild-type spike ($\Delta G_{e\text{-isolated}}$; Figure 2). The ΔG_e values reflect a major part of the energy contribution of each residue to the overall folding free energy. Its absolute difference between the isolated and complex states ($|\Delta\Delta G_e|$) indicates the importance of the residue in spike/ACE2 binding. We used two arbitrary criteria to identify key residues: (1) the energy contributions in both isolated and complex are large enough ($\Delta G_{e\text{-complex}} < -1.0$ kcal/mol and $\Delta G_{e\text{-isolated}} < -1.0$ kcal/mol); or (2) the absolute energy difference between isolated and complex is large enough ($|\Delta\Delta G_e| > 1.0$ kcal/mol). According to the criteria, all key residues fall in the unshaded region in Figure 2. These key residues are divided into four groups.

2.3.1 | Mutations that decrease the spike's structural stability and weaken the spike/ACE2 binding affinity

K417N has been found in the beta, gamma, and delta variants, which reduced spike/ACE2 binding affinity by 3-fold[63–66] by destroying ionic interactions.[29,43,44] K417 locates at the spike/ACE2 interface and is surrounded by several charged residues of both ACE2 and spike (Figure 3A). These charged residues from ACE2 include both positive (K26, K31, H34) and negative (D30, E37, E38) residues but forming a local electronegative region. Our calculations confirmed a strong positive electrostatic contribution in spike/ACE2 complex with ΔG_e = 2.92 kcal/mol. K417 may have intramolecular electrostatic interactions with spike's E406. The mutation may destroy it and result in the destabilization of spike.

2.3.2 | Mutations that increase the structural stability of the isolated spike

The five mutations to Lysine (T547K, N679K, N764K, N856K, N969K) give large negative ΔG_e contributions of in both the spike/ACE2 complex and the isolated spike (Figure 2). Because these residues are located outside the RBD, these mutations affect the stability of the isolated spike protein itself rather than the spike/ACE2 complex binding pattern. Our calculations indicate that these five mutations result in the largest value of ΔG_2 among all individual mutations (Table S1), which is consistent with the conclusion from the energy contribution analyzation (Figure 2). We also checked the electrostatic environment around these sites and found there was at least one negative residue interacting with Lysine nearby each site (Figure 3). The five mutations may enhance these interactions occur either within a single chain (Figure 3C,D) or between multichains of the spike protein (Figure 3B,E,F). These interactions may help spike trimer's subunits bind tightly. For example, two positive residues (R995 and R1000) near N969 interact with corresponding negative residues (D427 and D428; Figure 3F). The N969K mutation may introduce a new interaction between K969 and D428 (Figure 3F). For validation, we removed these interactions from the omicron variant by mutating the

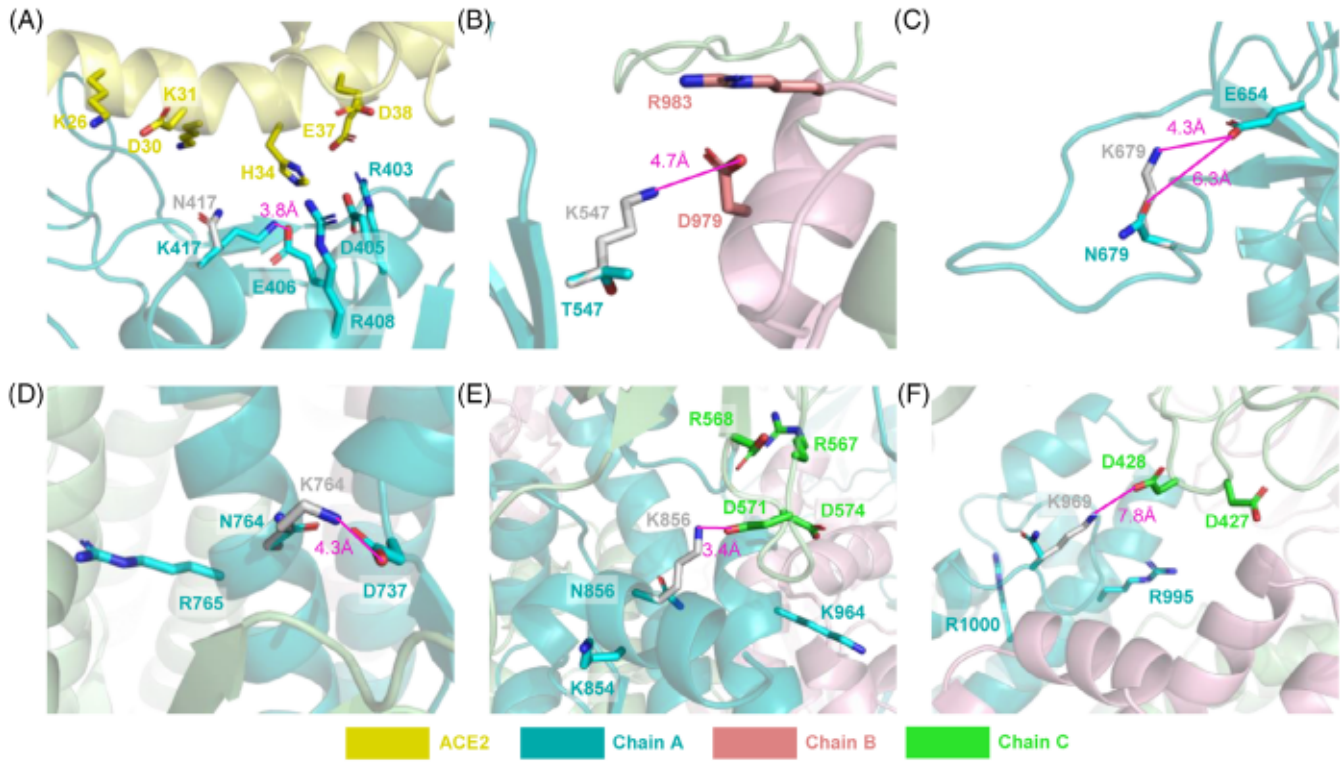

FIGURE 3 Structural representation of the position and the electrical environment of (A) K417N, (B) T547K, (C) N679K, (D) N764K, (E) N856K, and (F) N969K. The magenta lines and texts indicate the distances of key interactions.

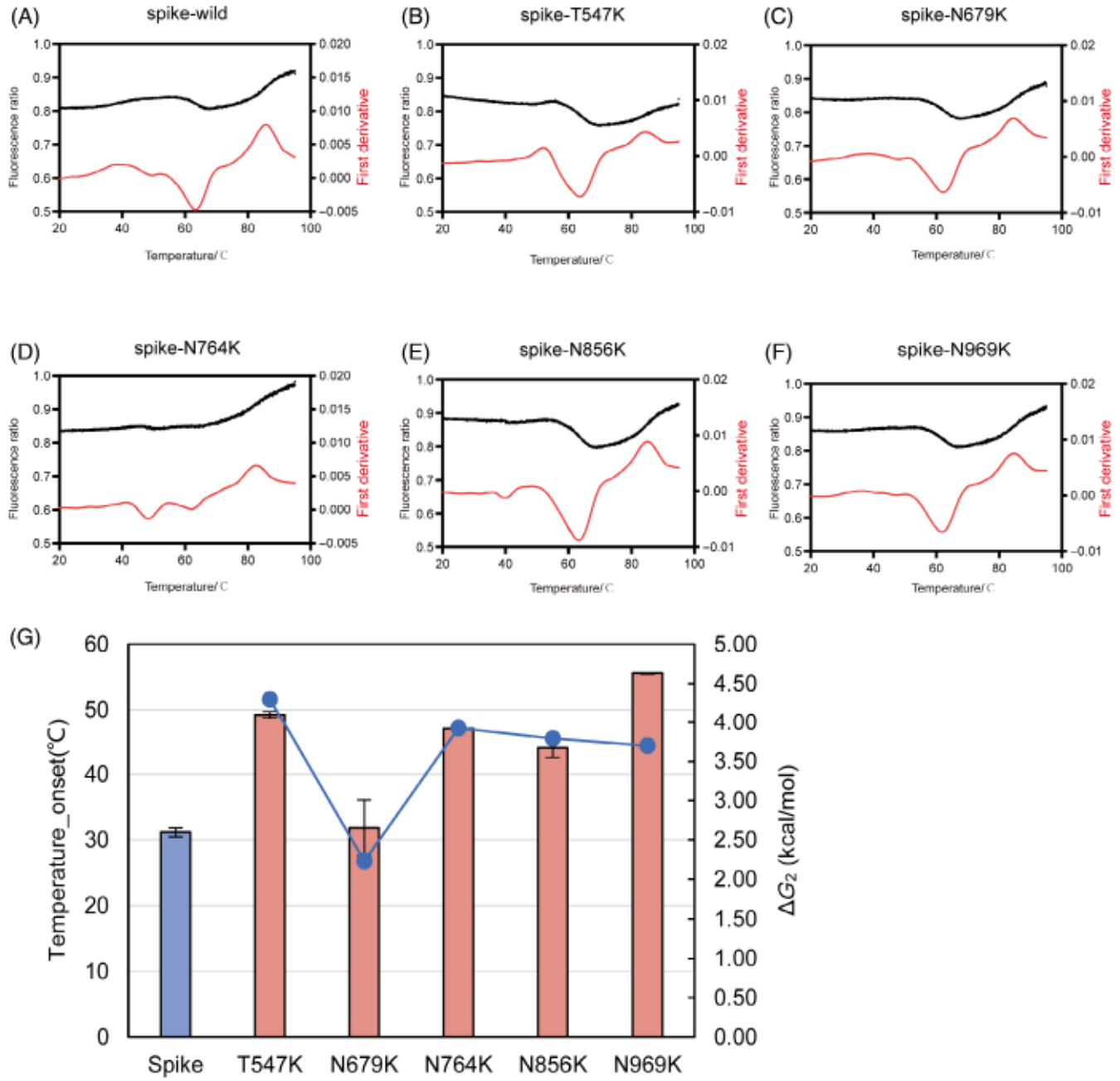

FIGURE 4 The experimental results of isolated spike structural stability. (A–F) The thermal stability of spike protein wild type (WT) and mutants using the nanoDSF method. All spike proteins were in the PBS buffer and the test concentrations were 0.2 mg/mL. The test temperature starts at 20°C and rises 1 degree per minute until it reaches 95°C. the peaks of the first derivative represent the protein started unfolding. (G) The onset temperature of protein unfolding (Temperature_onset) of the isolated wild-type spike protein and mutants. The bar represents the onset temperatures, which were measured by using the nanoDSF method. The data are shown as mean ± SEM based on three experiments. The points and line in blue represent the ΔG2 of each mutant in our calculations.

corresponding charged residues to alanine. The result showed that the spike protein's structural stability decreased ($\Delta G_2 = -2.97$ kcal/mol). We also performed thermal stability detecting experiments to verify the mutational effects (Figure 4A–F). The results showed that the mutated spike proteins started unfolding at a higher temperature. Temperature_onset represents the temperature that a testing protein starts to unfold, which reflects the thermal stability of the testing protein. The experimental results show that all onset temperatures of protein with the five mutations is higher than that of wild-type spike protein, indicating the structural stabilities of mutated spike increased (Figure 4G and Table S5). The proteins used for thermal stability detecting were verified by SDS-PAGE electrophoresis. (Figure S4). The experimental results also have a similar trend with the calculation of ΔG_2 (defined in Equation 3), which confirm the accuracy of our

calculations. Both the calculated and experimental results confirmed the five mutations to lysine indeed enhance the binding by introducing new electrostatic interactions to increase the overall protein structural stability.

2.3.3 | Potential mutation sites that reduce the structural stability of the spike

There are two residues, E583 and D663, which also give negative contribute to the spike's structural stability with $\Delta G_e = -1.11$ and -1.28 kcal/mol, respectively. But they never mutated in any major variant of SARS-CoV-2. The E583D mutations only occurred in some Indian variants with low frequency.[67] The D663 has been reported for having electrostatic interaction with the cleavage residue R685 to strongly stabilize the R685's position and facilitating the recognition by the protease.[68] In this work, we mutated these two sites into alanine and calculated their binding free energy change. It was found that ΔG_2 is -2.03 and -3.9 kcal/mol for E583A's and D663A's, respectively. This suggests that substituted by alanine indeed destabilize the spike protein. These two residues may be potential mutational sites for novel viral mutants in the future.

2.3.4 | Mutations that enhance the spike/ACE2 binding affinity

The four mutations (N440K, T478K, Q493R, and Q498R) are all located at the receptor binding motif of RBD, which are directly involved in the binding with ACE2. They also show remarkable binding energy change with $\Delta\Delta G = -3.93$ kcal/mol for N440K, $\Delta\Delta G = -4.96$ kcal/mol for T478K, $\Delta\Delta G = -3.01$ kcal/mol for Q493R, and $\Delta\Delta G = -1.42$ kcal/mol for Q498R (Figure 1 and Table S1). The ΔG_e of these mutations show a large negative contribution of ΔG_e in spike/ACE2 complex (-1.58, -1.47, -0.6 and -0.9 kcal/mol) but not in the isolated spike protein (-0.29, -0.21, 1.19, and 0.56 kcal/mol), implying that these mutations destabilized spike's structural stability but enhance the interactions between ACE2 and the spike.

The four mutations in omicron were all mutated to positively charged residues that facilitate the interaction with nearby negative charged residues of ACE2. We calculated the surface potential distributions of omicron and wild-type RBD and plotted their electrostatic potential surfaces by using APBS tool[69] (Figure 5A). The RBD/ACE2 interface is composed by two components with opposite potentials: the negative ACE2 surface (Figure S1) and the positive RBD surface of spike (Figure 5A). The positive potential of the omicron RBD surface towards ACE2 is significantly stronger than that of the wild type (Figure 5A). There are several charged residues of ACE2 around these four mutations (Figure 5B). The number of negative residues is much larger than positive (7 vs. 2), thus a negative potential is formed on the ACE2 surface.

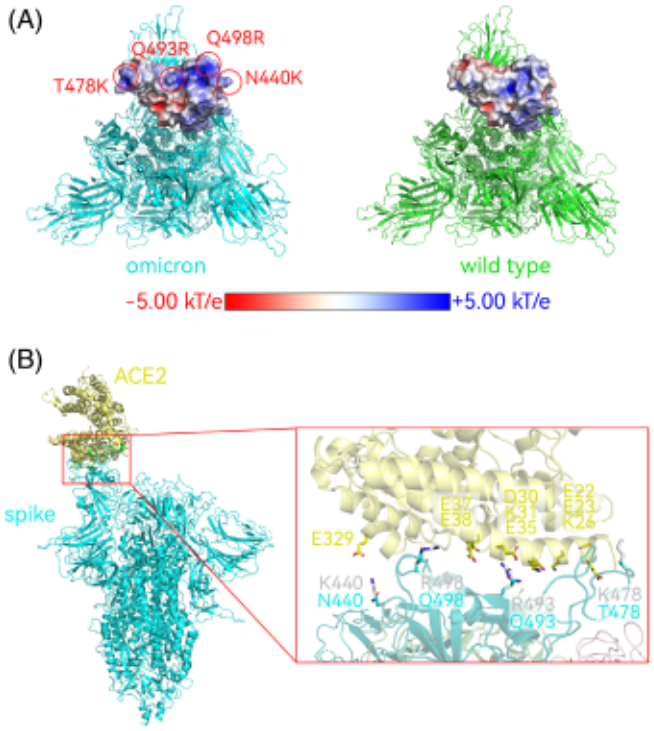

FIGURE 5 The visualization of spike receptor-binding domain/angiotensin-converting enzyme-2 (RBD/ACE2) interface and the experimental binding affinity of RBD/ACE2. (A) The electrostatic potential surface was calculated by APBS of the omicron variant RBD and the wild-type RBD. (B) The locations of N440K, T478K, Q493R, and Q498R in the RBD and the interacting residues of ACE2; Yellow texts mark the charge residues of ACE2, blue texts mark the residues of RBD before mutation, and gray texts marks the residues of RBD after mutation.

We performed biolayer interferometry (BLI) technology experiments to examine the mutational effect on spike/ACE2 binding (Figure 6A–F). The experimental results show the K_d values of the four mutated spike protein/ACE2 are significantly lower than wildtype (Figure 6G). The K_d values of Q493R and ALL have been sufficiently low, approaching 0, with average K_d values of 0.01 and 0.12, indicating a tight binding between spike proteins carrying these mutations and the ACE2 receptor. These results indicated the binding affinities increase because of these mutations. The proteins used for the BLI were verified by SDS-PAGE electrophoresis. (Figure S4). A scatter plot of experimental versus computed $\Delta\Delta G_{binding}$ values is given in Figure 6H. The data points are colored based on the mutation and shaped based on data source (solid squares for simulated results and hollow squares for experimental ones). The trend of $\Delta\Delta G_{binding}$ converted from the experimental K_d values agree well with our calculations (Figure 6H). The K_d value of the protein with four mutations is 0.12 nM, which is higher than single-site mutant Q493R (0.04 nM) but lower than N440K (2 nM), T478K (0.08 nM), and Q498R (3.54 nM). This confirmed the epistasis effect of mutations and could lead us to consider the combined effect of multiple mutations sites when designing therapeutic antibody for the virus. Apparently, the

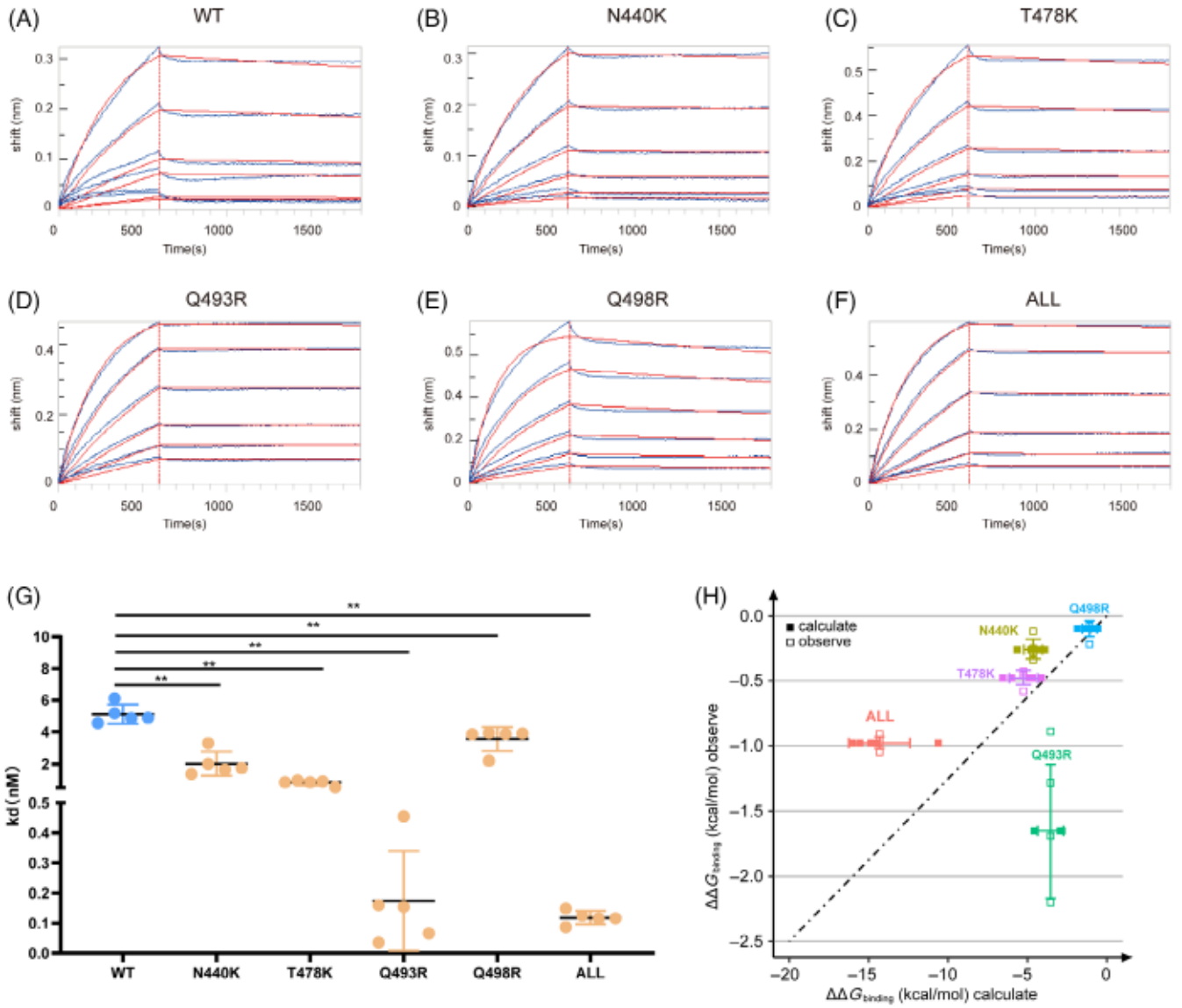

FIGURE 6 The experimental results of spike/angiotensin-converting enzyme-2 (ACE2) binding affinity. (A–F) The biolayer interferometry sensorgrams display the binding between ACE2 and spike protein (WT and different mutants). The data are shown as blue lines, and the best fit of the data to a 1:1 binding model is shown in red.(G) K_d values of Spike protein WT and mutants. Equilibrium dissociation constants (K_d) were obtained from k_{off}/k_{on} (Table S3). The data are shown as box plots of five repeats (the dots). The center, lower and upper lines in each box indicate the median, the first quartile, and the third quartile, respectively. The significances of difference between each mutant and wild type were performed by single-side Wilcox test. (H) Scatter plot of experimental and calculated $\Delta\Delta G_{binding}$ for spike protein mutants. Different mutants are represented by different colors. The solid squares "calculate" designates the computational results, whereas the hollow squares "observe" represent the experimental results. Error bars show the SEM.

calculated binding affinities overestimate the corresponding observed values in a major way. This overestimation is similar to what was found in our previous study.[36] This reflects insufficient dielectric compensation for the formation of an ionized side chain of lysine inside the protein,[70] because the Lysin residues find a way to increase their solvation by going to water. In our calculation, this dielectric compensation is adjusted by changing the dielectric constant in Equation (4). We have tested the optimal dielectric constant combination based on the previously obtained free energy change data of four mutations (see Section 4). The results also showed that calculations involving Lys mutations were more likely to be overestimated (Figure S3).

It is important to highlight the presence of several significant mutations, namely G142D, G339D, and D614G, which do not fail into the previously mentioned groups. Recent studies have suggested that G142D and G339D might impact the neutralizing ability of certain antibodies, thereby enhancing the omicron variant's immune escape ability.[71,72] However, our calculations indicate that these two mutations do not make a substantial contribution to the structural stability of the isolated spike protein or the spike/ACE2 complex (G142D: $\Delta G_{e\text{-complex}} = 0.37$, $\Delta G_{e\text{-isolated}} = -0.48$; G339D: $\Delta G_{e\text{-complex}} = 1.38$, $\Delta G_{e\text{-isolated}} = 0.94$; Figure 2). This information suggests that their impact on overall stability is limited. On the other hand, the D614G

mutation plays a pivotal role in numerous VOCs and is associated with a selective advantage.[25,73] Previous research has demonstrated that the D614G mutation enhances viral entry efficiency by improving ACE2 binding affinity through providing conformational flexibility to the spike trimer's overall structure.[26] It is worth noting that this enhancement is not directly attributable to increased spike-ACE2 interaction, as D614 is located in the SD1/2 region rather than the RBD region (Figure 1). Rather, it is driven by the heightened structural stability of the spike/ACE2 complex. Our calculations further confirm this observation (D614G: $\Delta G_{\text{e-complex}} = -0.87$, $\Delta G_{\text{e-isolated}} = -0.73$; Figure 2). In summary, our investigation sheds light on the limited impact of G142D and G339D on structural stability, while emphasizing the crucial role of the D614G mutation in VOCs. These findings contribute to our understanding of the omicron variant's behavior and potential immune escape mechanisms.

2.4 | Weaker affinities to most antibodies

The omicron variant has five sublineages, BA.1, BA.2, BA.3, BA.4, and BA.5. BA.1 is the lineage we studied above. BA.2 and BA.3 share 31 identical mutations with BA.1 on the spike protein, but have 18 and 11 distinct ones on the spike protein, respectively.[74] BA.4 and BA.5 have the same mutations on spike protein and they share 21 spike mutations with BA.1. BA.2 has an "increased growth rate" in comparison with BA.1.[75] The $\Delta\Delta G$ of these omicron sublineages to ACE2 suggested that BA.2, BA.3, and BA.4 do not present higher ACE2 binding affinity than BA.1 (Table S3). Moreover, we calculated the mutational $\Delta\Delta G$ of these lineages to several antibodies and found BA.1 shows weaker binding affinity to most antibodies except for S309, which is consistent with experimental observations.[15,76] BA.2 binds more tightly to most antibodies except for LY-CoV555. The $\Delta\Delta G$ of BA.3 to antibodies CT-P59, AZD1061, and LY-CoV555 is more positive than that of BA.1 (Table S3), indicating greater interference with the spike/antibody interactions and possible stronger immune evasion. BA.4 exhibits a stronger spike/antibody affinity reduction effect than the other three sublineages (Table S3) implying it may have the strongest immune evasion ability.[77] These analyses suggested that, in addition to gaining strong ACE2 affinity, the omicron variant has larger immune evasion ability to further enhance its transmission ability.

3 | DISCUSSION

Extending our previous studies,[51,55] we used the same CG model to overcome the challenge of analyzing the energetics of the omicron/ACE2 complex. Our results indicated that the omicron variant enhances its binding affinity to ACE2 and structural stability of isolated spike. Furthermore, we identified key mutations contributing to the free energy change by different mechanisms. The enhanced electrostatic interactions of Q493R and Q498R found in our study is consistent with the conclusions in other studies.[21,30,78,79] Moreover, our results also discovered some key mutations, such as N440K that enhances the spike/ACE2 binding and the five mutations to Lysine increase the spike protein's structural stability. This important finding reflects the fact that our evaluation is based on the perspective of energy and not only on observing structure. The method allowed us to investigate the effects of mutations on the entire system.

Because our calculations are based on the entire system model of spik-ACE2, we conducted wet experiments to express and purify full-length spike trimers, instead of solely focusing on the RBD as in most studies.[27,28] Purifying the full-length spike trimer proved challenging due to its extensive size, with over 3500 residues. After several trial-and-error attempts, we successfully identified the optimal condition for purifying this protein, which involved elution with 300 mM imidazole twice. To assess the binding affinity of the spike protein with the ACE2 receptor, similar to previous studies,[80–82] we employed the BLI experiment. The method measures kinetics and biomolecular interactions based on wave interference. Additionally, we utilized NanoDSF, a reliable technique commonly employed to test the protein stability by utilizing intrinsic tryptophan or tyrosine fluorescence. Many studies investigating spike protein stability have utilized this approach.[83–85] Therefore, in line with these methodologies employed in similar articles, we employed the BLI experiments and NanoDSF technique to validate our calculations.

Understanding the underlying mechanism of the reduced lethality of the omicron variant is a vital question.[18] A possible explanation is related to the pathway of virus entry after spike binding to ACE2 receptor. Two possible pathways exist for coronavirus entry into cells: the TMPRSS2 pathway and the endocytic pathway.[86]

The TMPRSS2 pathway depends on the transmembrane protease, serine 2, which colocalizes with ACE2 at the cell membrane and processes the SARS-CoV-2 Spike protein to enable virus-host membrane fusion.[87] Earlier SARS-CoV-2 VOCs prefer to the TMPRSS2 pathway, by which the spike protein is cleaved at the S1/S2 sites by TMPRSS2 that leads to dissociation of S1 and S2 subunits. Then, the S2 subunit undergoes a large conformational rearrangement to bind with the host cell membrane and viral entry of the host cell.[88] The energy barrier of the process may be increased for the omicron variant because the omicron/ACE2 complex is much more stable, and this results in lower viral lethality.

However, some researchers suggested the omicron variant abandon the TMPRSS2 pathway in favor of the endocytic pathway, by which the virus is swallowed by host cells through endocytosis.[89,90] Due to the lower protein level of ACE2 and the higher level of TMPRSS2 in the lungs than in the upper airways,[91,92] the omicron variant has more difficulties in infecting the lungs than the nose or the throat.[93,94] Therefore, the mutated virus cannot fuse individual lung cells together into larger blobs called syncytia and thus cannot cause severe illness.

To further elaborate on the above issue, we note that the omicron spike protein has activated more slowly.[95] In considering this effect, we noticed that in order to bind to ACE2, the spike must undergo a conformational transition to an activated conformation. The conformation conversion is facilitated by the presence of ACE2.[88]

Zhang et al.[30] found that the omicron variant spike protein requires a higher level of ACE2 concentration than other variants. In this case, even though the binding affinity of ACE2 is enhanced, the omicron variant is still hard to invade human cells massively and cause severe symptom, especially in lung cells with low ACE2 expression.[91,92]

Our study of the affinity of the omicron lineages to several antibodies is consistent with the greater interference with the spike/antibody interactions and stronger immune evasion.

It is worth noting that the mutational effects of the SARS-CoV-2 spike protein extend beyond its affinity with ACE2. Recent studies have shown that the spike protein can also interact with human monoamine oxidases (MAO) with affinities that are comparable to those with the ACE2 receptor. MAO enzymes play important roles in the metabolic clearance and regulation of brain amine levels, such as the neurotransmitters dopamine and serotonin. The formation of MAO/spike protein complexes modifies MAO affinity for its neurotransmitters, which leads to imbalances in their levels and potentially contributes to neurological illnesses following virus infection. Moreover, it is suggested that more contagious virus variants could cause larger disturbances of MAO and lead to more severe neurological illnesses.[96] These findings underscore the complex and profound mutational effects on the pathogenicity of the SARS-CoV-2 virus in addition to its interaction with ACE2. Therefore, it is imperative to continuously monitor and track emerging mutations and viral variants to better understand their impact on disease severity and inform public health interventions.

Glycosylation of spike proteins and ACE2 receptors is essential factor to consider when discussing their interactions. The spike trimer has been discovered to contain numerous glycosylation sites, with ~40% of the protein being shielded by glycans.[97] Since cryo-EM and x-ray crystallography are unable to accurately determine glycan composition, computational simulation has emerged as a vital tool for studying the glycosylation of spike protein.[98,99] Glycans impact the spike/ACE2 binding in three primary ways: first, they influence the down-to-up dynamics of spike conformation[32,100]; second, they alter glycan-protein or glycan–glycan interactions[101,102]; and third, they modify the interface by either shielding binding sites or displacing the binding residues.[103,104] However, current methods are unable to fully elucidate the role of glycosylation. For instance, both computational and experimental studies have demonstrated that the glycosylation of N165, N234, and N343 benefits spike/ACE2 binding.[32,105] Surprisingly, recent experiments have shown that the nature of the glycans at N234, N165, and N343 does not affect the binding affinity of the spike protein to the ACE2.[106] These findings highlight the importance of glycosylation in understanding spike protein behavior, but due to its complexity, further optimization of our research tools is still necessary.

In summary, we suggest that the increased transmissibility and reduced lethality can be rationalized by our calculations. The reduced lethality could be originated from the possibility that the variant adopts an alternative unique host cell entry pathway that makes it harder to infect the lung cells. The increased transmissibility is mainly accounted for by the enhanced spike/ACE2 binding affinity, improved immune evasion, and weaker binding to inhibitor. Studying the molecular mechanisms that enable these approaches may help us find ways to deal with variant viruses in advance.

4 | METHODS

4.1 | Modeling the complex structures

The wild-type spike/ACE2 complex structure was taken from the high-resolution cryo-EM structure with PDB ID: 7DF4.[88] Structural data showed that the RBD of omicron variant's spike has no significant conformational change compared with the wild type.[21] We believe that using the original wild-type structure as the first-order approximation in predicting mutational effects here is the best option. One of missing fragments (Q677-A688) in the experimental structure was repaired by using Modeller,[107] because two mutations (N679K and P681H) locate in the fragment. The mutations were introduced into wild-type spike protein by using PyMOL. Removing the ACE2 receptor from the complex structure, we obtained the isolated spike protein structure. The structures of antibodies and their interactive model were extracted from known structures: CT-P59 (PDB ID: 7CM4), AZD1061 (PDB ID: 7L7E), LY-CoV555 (PDB ID: 7KMG), and S309(PDB ID: 7TN0; see "Constructing protein models" in the Supplementary information S1).

4.2 | Calculating the CG free energy

First, we relax the protein at 50 K 0.1 ns in the all-atomic model. Then the AA structures were converted into CG representation (Figure S2) and performed extensive (5000 steps, 0.001 ps step-size) relaxation under 50 K temperature until the energy of system is converged. During relaxation, one structure was output each 100 steps and finally, we got a conformational trajectory composed of 50 structures. All these structures would be used for energy evaluation. The CG model we used[52–54] focuses on the precise treatment of the electrostatic and is sensitive to the charge distribution of the protein ionized groups. In consequence, before energy evaluation, a MCPT method[52] was used to determine the charge states of the residues in each structure. During MCPT, protons were "jumped" between ionizable residues, and a standard Metropolis criterion was utilized to calculate the acceptance probability. The total CG energy was calculated according to the following formula:

$$\begin{aligned}\Delta G_{fold} &= \Delta G_{main} + \Delta G_{side} + \Delta G_{main-side}\# \\ &= c_1\Delta G_{side}^{vdw} + c_2\Delta G_{solv}^{CG} + c_3\Delta G_{HB}^{CG} + \Delta G_{side}^{elec} + \Delta G_{side}^{polar} \\ &+ \Delta G_{side}^{hyd} + \Delta G_{main-side}^{elec} + \Delta G_{main-side}^{vdw}\end{aligned} \quad (1)$$

The terms on the right are the side chain van der Waals energy, main chain solvation energy, main chain hydrogen bond energy, side chain electrostatic energy, side chain polar energy, side chain hydrophobic energy, main chain/side chain electrostatic energy, and main

chain/side chain van der Waals energy, respectively. The scaling coefficients $c1$, $c2$, and $c3$ are taking values of 0.10, 0.25, and 0.15 in this work. (See "The energetics of the CG protein model" in the Supplementary information S1).

Due to the large size of the protein, after 1000 steps, the energy reached equilibrium but fluctuates. Therefore, the average energy of the last 15 structures was used as the final energy. All relative calculations were performed using the Molaris-XG package.[108,109]

4.3 | Calculating the binding free energy changes

The binding energies for spike/ACE2 are defined as follows.

$$\Delta G_{binding} = G_{spike-ACE2} - G_{ACE2} - G_{spike} \tag{2}$$

For the mutated binding free energy change of spike/ACE2 complex:

$$\begin{aligned}\Delta\Delta G_{binding} &= \Delta G_{binding_{mutant}} - \Delta G_{binding_{WT}}\# \\ &= \left(G_{ACE2-spike_{mutant}} - G_{spike_{mutant}} - G_{ACE2}\right) \\ &\quad - \left(G_{ACE2-spike_{WT}} - G_{spike_{WT}} - G_{ACE2}\right) \\ &= \left(G_{ACE2-spike_{mutant}} - G_{ACE2-spike_{WT}}\right) \\ &\quad + \left(G_{spike_{WT}} - G_{spike_{mutant}}\right) \\ &= \Delta G_1 + \Delta G_2\end{aligned} \tag{3}$$

4.4 | Evaluating the electrostatic effect

We implicitly incorporate the effect of the structural change in the subsequent energy calculation by adjusting the effective dielectric constant. In previous studies, we noticed that the underestimation of the dielectric compensation effect led to an overestimation of our free energy calculations.[55] In our CG model, the dielectric compensation effect was mainly related to the dielectric constant. The dielectric constant was calculated by the function:

$$\varepsilon_{eff} = 1 + \varepsilon'\left[1 - \exp\left(-\mu r_{ij}\right)\right] \tag{4}$$

where ε' is a statistical mechanical dielectric constant, r_{ij} is the distance of two ionized groups, and μ is a scaling coefficient for the distance. The magnitude of ε' reflects the compensation of the unscreened interaction by the protein and water reorganization.[110–112] Refer to the experimental value of $\Delta\Delta G$ of four mutations (E484K, F486L, Q493N, Q498Y), we tested the influence of different effective dielectric constants in the CG model, with ε' in range [20, 80]; μ in range [0.2,1.2] (Figure S3). The optimal value that minimized the difference between calculational and experimental values was obtained with $\varepsilon' = 80$ and $\mu = 0.6$ and used here (see "Testing the dielectric constant" in the Supplementary information S1).

4.5 | Cloning and expression of spike, spike mutants, and ACE2

The mammalian cell codon-optimized nucleotide sequence coding for the spike protein of the SARS-CoV-2 and ACE2 of the human was synthesized commercially (Genewiz, Suzhou, China). The spike protein in this paper is soluble and only includes the amino acids from 1 to 1213. The soluble version of spike alone with C-terminal thrombin cleavage site, T4 foldon trimerization domain, and 6× His tag was cloned into pCAGGS vector. The spike protein sequence was modified to remove the polybasic cleavage site (RRAR to A), and two stabilizing mutations were introduced as well (K986P and V987P). The ACE2, including a C-terminal FC tag, was cloned into pcDNA3.1 vector. The spike mutants were gotten by overlap polymerase chain reaction that used wild-type spike as template with specific mutagenic primers (Table S4). Then these expression vectors were transfected into HEK293F cell with polyethylenimine. After 5 days, the target proteins were purified from the cell culture supernatant.

4.6 | Protein purification

The HEK293F culture supernatant was collected by centrifugation at 2000 rpm for 5 min. Then the supernatant was filtered with 0.22 μM filter and was purified by the Ni-NTA resin affinity chromatography. First, the Ni chromatography column was balanced by PBS (PH = 7.4). Then the supernatant is flowed through the Ni column at a speed of 0.5 mL/min. Finally, the Ni column was washed by the 300 mM imidazole and the imidazole was collected. The collected imidazole was dialyzed in PBS at 4°C overnight, so the protein was eluted in the PBS. All proteins were verified by the SDS-PAGE electrophoresis (Figure 5A,D).

4.7 | Spike protein thermal stability analysis

The thermal stability of spike protein and spike mutants was detected by the Prometheus NT.48 (NanoTemper) through the nanoDSF technology. All of the proteins were adjusted to a same concentration of 0.2 mg/mL with PBS buffer. Aspirate the protein sample for ~10 μL using a capillary tube. All of the proteins were detected at the same time. The range of thermal stability testing temperature is 20–95°C. The onset temperature of protein unfolding (Temperature_onset) of spike protein and spike mutants were detected as the indicator of protein thermal stability (Figure 5B).

4.8 | Spike protein/ACE2 binding

The binding of Spike protein and mutants with ACE2 was detected by the Octet RED96e System (ForteBio) through BLI technology. The ACE2 protein with FC tag was immobilized to a protein A sensortip. Then, the sensortip was dipped into the wild-type spike protein and

spike mutants to measure the association between ACE2 and spike/spike mutants (k_{on}). After that, the sensortip was dipped into the well with dilution buffer (1 × PBS, pH 7.4, with 0.1% BSA and 0.02% Tween-20) to measure the dissociation (k_{off}). The data analysis was done by the Octet Data Analysis HT software (Figure 5E). Equilibrium dissociation constants (K_d) were obtained from k_{off}/k_{on}.

AUTHOR CONTRIBUTIONS

Ke An: Investigation; methodology; visualization; writing—original draft; project administration; formal analysis; data curation. **Xianzhi Yang:** Methodology; formal analysis; investigation; visualization; writing—original draft; data curation. **Mengqi Luo:** Investigation; writing—original draft; methodology; visualization; formal analysis; data curation. **Junfang Yan:** Investigation; formal analysis. **Peiyi Xu:** Investigation; formal analysis. **Honghui Zhang:** Investigation; formal analysis. **Yuqing Li:** Writing—review and editing; resources; supervision. **Song Wu:** Funding acquisition; resources. **Arieh Warshel:** Funding acquisition; writing—review and editing; software; methodology; conceptualization; supervision. **Bai Chen:** Funding acquisition; writing—review and editing; project administration; methodology; conceptualization; validation; supervision.

ACKNOWLEDGMENTS

This work was supported by the National Institutes of Health R35 (GM122472), the National Science Foundation (grant no. MCB 2142727), 2021 Basic Research General Project of Shenzhen, China (grant no. 20210316202830001), the National Natural Science Foundation of China (grant no. 61931024), and Shenzhen Science and Technology Innovation Commission (grant no. RCJC20200714114557005), the Warshel Institute for computational Biology funding from Shenzhen City and Longgang District. We thank Dr. Danfeng Shi, Dr. Xiaohong Zhu, and Dr. Yue Zhang for discussion and article preparation.

PEER REVIEW

The peer review history for this article is available at https://www.webofscience.com/api/gateway/wos/peer-review/10.1002/prot.26663.

DATA AVAILABILITY STATEMENT

Data sharing is not applicable to this article as no datasets were generated or analysed during this study.

ORCID

Ke An https://orcid.org/0000-0002-2741-8269

REFERENCES

1. Aydogdu MO, Rohn JL, Jafari NV, Brako F, Homer-Vanniasinkam S, Edirisinghe M. Severe acute respiratory syndrome type 2-causing coronavirus: variants and preventive strategies. *Adv Sci (Weinh)*. 2022;9:e2104495. doi:10.1002/advs.202104495
2. Liu Y, Liu J, Plante KS, et al. The N501Y spike substitution enhances SARS-CoV-2 infection and transmission. *Nature*. 2022;602:294-299. doi:10.1038/s41586-021-04245-0
3. Chen RE, Zhang X, Case JB, et al. Resistance of SARS-CoV-2 variants to neutralization by monoclonal and serum-derived polyclonal antibodies. *Nat Med*. 2021;27:717-726. doi:10.1038/s41591-021-01294-w
4. Garcia-Beltran WF, Lam EC, St Denis K, et al. Multiple SARS-CoV-2 variants escape neutralization by vaccine-induced humoral immunity. *Cell*. 2021;184:2523. doi:10.1016/j.cell.2021.04.006
5. Liu Y, Liu J, Xia H, et al. Neutralizing activity of BNT162b2-elicited serum. *N Engl J Med*. 2021;384:1466-1468. doi:10.1056/NEJMc2102017
6. Wang P, Nair MS, Liu L, et al. Antibody resistance of SARS-CoV-2 variants B.1.351 and B.1.1.7. *Nature*. 2021;593:130-135. doi:10.1038/s41586-021-03398-2
7. Balint G, Voros-Horvath B, Szechenyi A. Omicron: increased transmissibility and decreased pathogenicity. *Signal Transduct Target Ther*. 2022;7:151. doi:10.1038/s41392-022-01009-8
8. Escalera A, Gonzalez-Reiche AS, Aslam S, et al. Mutations in SARS-CoV-2 variants of concern link to increased spike cleavage and virus transmission. *Cell Host Microbe*. 2022;30:373-387.e377. doi:10.1016/j.chom.2022.01.006
9. Ren SY, Wang WB, Gao RD, Zhou AM. Omicron variant (B.1.1.529) of SARS-CoV-2: mutation, infectivity, transmission, and vaccine resistance. *World J Clin Cases*. 2022;10:1-11. doi:10.12998/wjcc.v10.i1.1
10. Callaway E, Ledford H. How bad is omicron? What scientists know so far. *Nature*. 2021;600:197-199. doi:10.1038/d41586-021-03614-z
11. Kozlov M. How does omicron spread so fast? A high viral load isn't the answer. *Nature*. 2022. doi:10.1038/d41586-022-00129-z
12. Graham F. Daily briefing: omicron coronavirus variant puts scientists on alert. *Nature*. 2021. doi:10.1038/d41586-021-03564-6
13. Kupferschmidt K. Where did 'weird' omicron come from? *Science*. 2021;374:1179. doi:10.1126/science.acx9738
14. Cao Y, Wang J, Jian F, et al. Omicron escapes the majority of existing SARS-CoV-2 neutralizing antibodies. *Nature*. 2021;602:657-663. doi:10.1038/s41586-021-04385-3
15. Planas D, Saunders N, Maes P, et al. Considerable escape of SARS-CoV-2 omicron to antibody neutralization. *Nature*. 2021;602:671-675. doi:10.1038/s41586-021-04389-z
16. Flemming A. Omicron, the great escape artist. *Nat Rev Immunol*. 2022;22:75. doi:10.1038/s41577-022-00676-6
17. Nyberg T, Ferguson NM, Nash SG, et al. Comparative analysis of the risks of hospitalisation and death associated with SARS-CoV-2 omicron (B.1.1.529) and delta (B.1.617.2) variants in England: a cohort study. *Lancet*. 2022;399:1303-1312. doi:10.1016/S0140-6736(22)00462-7
18. Dance A. Omicron's lasting mysteries: four questions scientists are racing to answer. *Nature*. 2022;603:22-24. doi:10.1038/d41586-022-00428-5
19. Ou X, Liu Y, Lei X, et al. Characterization of spike glycoprotein of SARS-CoV-2 on virus entry and its immune cross-reactivity with SARS-CoV. *Nat Commun*. 2020;11:1620. doi:10.1038/s41467-020-15562-9
20. Zhang H, Penninger JM, Li Y, Zhong N, Slutsky AS. Angiotensin-converting enzyme 2 (ACE2) as a SARS-CoV-2 receptor: molecular mechanisms and potential therapeutic target. *Intensive Care Med*. 2020;46:586-590. doi:10.1007/s00134-020-05985-9
21. Yin W, Xu Y, Xu P, et al. Structures of the omicron spike trimer with ACE2 and an anti-omicron antibody. *Science*. 2022;375:1048-1053. doi:10.1126/science.abn8863
22. Wrapp D, Wang N, Corbett KS, et al. Cryo-EM structure of the 2019-nCoV spike in the prefusion conformation. *Science*. 2020;367:1260-1263. doi:10.1126/science.abb2507
23. Starr TN, Greaney AJ, Hilton SK, et al. Deep mutational scanning of SARS-CoV-2 receptor binding domain reveals constraints on folding

and ACE2 binding. *Cell*. 2020;182:1295-1310.e1220. doi:10.1016/j.cell.2020.08.012

24. Zahradnik J, Marciano S, Shemesh M, et al. SARS-CoV-2 variant prediction and antiviral drug design are enabled by RBD in vitro evolution. *Nat Microbiol*. 2021;6:1188-1198. doi:10.1038/s41564-021-00954-4
25. Khatri R, Siddqui G, Sadhu S, et al. Intrinsic D614G and P681R/H mutations in SARS-CoV-2 VoCs alpha, Delta, omicron and viruses with D614G plus key signature mutations in spike protein alters fusogenicity and infectivity. *Med Microbiol Immunol*. 2023;212:103-122. doi:10.1007/s00430-022-00760-7
26. Ozono S, Zhang Y, Ode H, et al. SARS-CoV-2 D614G spike mutation increases entry efficiency with enhanced ACE2-binding affinity. *Nat Commun*. 2021;12:848. doi:10.1038/s41467-021-21118-2
27. Zhou L, Liu T, Mo M, et al. Exploring the binding affinity and mechanism between ACE2 and the trimers of Delta and omicron spike proteins by molecular dynamics simulation and bioassay. *J Chem Inf Model*. 2022;62:4512-4522. doi:10.1021/acs.jcim.2c00881
28. Zheng B, Xiao Y, Tong B, et al. S373P mutation stabilizes the receptor-binding domain of the spike protein in omicron and promotes binding. *JACS Au*. 2023;3:1902-1910. doi:10.1021/jacsau.3c00142
29. McCallum M, Czudnochowski N, Rosen LE, et al. Structural basis of SARS-CoV-2 omicron immune evasion and receptor engagement. *Science*. 2022;375:864-868. doi:10.1126/science.abn8652
30. Zhang J, Cai Y, Lavine CL, et al. Structural and functional impact by SARS-CoV-2 omicron spike mutations. *Cell Rep*. 2022;39:110729. doi:10.1016/j.celrep.2022.110729
31. Hong Q, Han W, Li J, et al. Molecular basis of receptor binding and antibody neutralization of omicron. *Nature*. 2022;604:546-552. doi:10.1038/s41586-022-04581-9
32. Sztain T, Ahn SH, Bogetti AT, et al. A glycan gate controls opening of the SARS-CoV-2 spike protein. *Nat Chem*. 2021;13:963-968. doi:10.1038/s41557-021-00758-3
33. Zimmerman MI, Porter JR, Ward MD, et al. SARS-CoV-2 simulations go exascale to predict dramatic spike opening and cryptic pockets across the proteome. *Nat Chem*. 2021;13:651-659. doi:10.1038/s41557-021-00707-0
34. Sang P, Chen YQ, Liu MT, et al. Electrostatic interactions are the primary determinant of the binding affinity of SARS-CoV-2 spike RBD to ACE2: a computational Case study of omicron variants. *Int J Mol Sci*. 2022;23:14796. doi:10.3390/ijms232314796
35. Hie B, Zhong ED, Berger B, Bryson B. Learning the language of viral evolution and escape. *Science*. 2021;371:284-288. doi:10.1126/science.abd7331
36. Maher MC, Bartha I, Weaver S, et al. Predicting the mutational drivers of future SARS-CoV-2 variants of concern. *Sci Transl Med*. 2021;14:eabk3445.
37. Beguir K, Skwark MJ, Fu Y, et al. Early computational detection of potential high-risk SARS-CoV-2 variants. *Comput Biol Med*. 2023;155:106618. doi:10.1016/j.compbiomed.2023.106618
38. Glasgow A, Glasgow J, Limonta D, et al. Engineered ACE2 receptor traps potently neutralize SARS-CoV-2. *Proc Natl Acad Sci U S A*. 2020;117:28046-28055. doi:10.1073/pnas.2016093117
39. Higuchi Y, Suzuki T, Arimori T, et al. Engineered ACE2 receptor therapy overcomes mutational escape of SARS-CoV-2. *Nat Commun*. 2021;12:1-13.
40. Remesh SG, Merz GE, Brilot AF, et al. Computational pipeline provides mechanistic understanding of omicron variant of concern neutralizing engineered ACE2 receptor traps. *Structure*. 2023;31:253-264.e256. doi:10.1016/j.str.2023.01.009
41. Havranek B, Lindsey GW, Higuchi Y, et al. A computationally designed ACE2 decoy has broad efficacy against SARS-CoV-2 omicron variants and related viruses in vitro and in vivo. *Commun Biol*. 2023;6:513. doi:10.1038/s42003-023-04860-9
42. Wu J, Zhang HX, Zhang J. In silico design of miniprotein to inhibit SARS-CoV-2 variant omicron spike protein. *Phys Chem Chem Phys*. 2023;25:14711-14725. doi:10.1039/d3cp01167d
43. Cai Y, Zhang J, Xiao T, et al. Structural basis for enhanced infectivity and immune evasion of SARS-CoV-2 variants. *Science*. 2021;373:642-648. doi:10.1126/science.abi9745
44. Gobeil SM, Janowska K, McDowell S, et al. Effect of natural mutations of SARS-CoV-2 on spike structure, conformation, and antigenicity. *Science*. 2021;373:eabi6226. doi:10.1126/science.abi6226
45. Zhang J, Xiao T, Cai Y, et al. Membrane fusion and immune evasion by the spike protein of SARS-CoV-2 Delta variant. *Science*. 2021;374:1353-1360. doi:10.1126/science.abl9463
46. Huang KA, Chen X, Mohapatra A, et al. Structural basis for a conserved neutralization epitope on the receptor-binding domain of SARS-CoV-2. *Nat Commun*. 2023;14:311. doi:10.1038/s41467-023-35949-8
47. Saville JW, Mannar D, Zhu X, et al. Structural analysis of receptor engagement and antigenic drift within the BA.2 spike protein. *Cell Rep*. 2023;42:111964. doi:10.1016/j.celrep.2022.111964
48. Gobeil SM, Janowska K, McDowell S, et al. D614G mutation alters SARS-CoV-2 spike conformation and enhances protease cleavage at the S1/S2 junction. *Cell Rep*. 2021;34:108630. doi:10.1016/j.celrep.2020.108630
49. Lu M, Uchil PD, Li W, et al. Real-time conformational dynamics of SARS-CoV-2 spikes on virus particles. *Cell Host Microbe*. 2020;28:880-891.e888. doi:10.1016/j.chom.2020.11.001
50. Yang Z, Han Y, Ding S, et al. SARS-CoV-2 variants increase kinetic stability of open spike conformations as an evolutionary strategy. *MBio*. 2021;13:e0322721. doi:10.1128/mbio.03227-21
51. Bai C, Warshel A. Critical differences between the binding features of the spike proteins of SARS-CoV-2 and SARS-CoV. *J Phys Chem B*. 2020;124:5907-5912. doi:10.1021/acs.jpcb.0c04317
52. Vorobyov I, Kim I, Chu ZT, Warshel A. Refining the treatment of membrane proteins by coarse-grained models. *Proteins*. 2016;84:92-117. doi:10.1002/prot.24958
53. Lee M, Kolev V, Warshel A. Validating a coarse-grained voltage activation model by comparing its performance to the results of Monte Carlo simulations. *J Phys Chem B*. 2017;121:11284-11291. doi:10.1021/acs.jpcb.7b09530
54. Vicatos S, Rychkova A, Mukherjee S, Warshel A. An effective coarse-grained model for biological simulations: recent refinements and validations. *Proteins*. 2014;82:1168-1185. doi:10.1002/prot.24482
55. Bai C, Wang J, Chen G, et al. Predicting mutational effects on receptor binding of the spike protein of SARS-CoV-2 variants. *J Am Chem Soc*. 2021;143:17646-17654. doi:10.1021/jacs.1c07965
56. McCallum M, de Marco A, Lempp FA, et al. N-terminal domain antigenic mapping reveals a site of vulnerability for SARS-CoV-2. *Cell*. 2021;184:2332-2347.e2316. doi:10.1016/j.cell.2021.03.028
57. Callaway E. Omicron likely to weaken COVID vaccine protection. *Nature*. 2021;600:367-368. doi:10.1038/d41586-021-03672-3
58. Kim I, Warshel A. Analyzing the electrogenicity of cytochrome c oxidase. *Proc Natl Acad Sci U S A*. 2016;113:7810-7815. doi:10.1073/pnas.1608118113
59. Lee M, Bai C, Feliks M, Alhadeff R, Warshel A. On the control of the proton current in the voltage-gated proton channel Hv1. *Proc Natl Acad Sci U S A*. 2018;115:10321-10326. doi:10.1073/pnas.1809766115
60. Bai C, Warshel A. Revisiting the protomotive vectorial motion of F0-ATPase. *Proc Natl Acad Sci U S A*. 2019;116:19484-19489. doi:10.1073/pnas.1909032116
61. Alhadeff R, Warshel A. A free-energy landscape for the glucagon-like peptide 1 receptor GLP1R. *Proteins*. 2020;88:127-134. doi:10.1002/prot.25777

62. Bai C, Asadi M, Warshel A. The catalytic dwell in ATPases is not crucial for movement against applied torque. *Nat Chem*. 2020;12:1187-1192. doi:10.1038/s41557-020-0549-6
63. Collier DA, de Marco A, Ferreira IATM, et al. Sensitivity of SARS-CoV-2 B.1.1.7 to mRNA vaccine-elicited antibodies. *Nature*. 2021;593:136-141. doi:10.1038/s41586-021-03412-7
64. McCallum M, Walls AC, Sprouse KR, et al. Molecular basis of immune evasion by the Delta and kappa SARS-CoV-2 variants. *Science*. 2021;374:1621-1626. doi:10.1126/science.abl8506
65. Thomson EC, Rosen LE, Shepherd JG, et al. Circulating SARS-CoV-2 spike N439K variants maintain fitness while evading antibody-mediated immunity. *Cell*. 2021;184:1171-1187.e1120. doi:10.1016/j.cell.2021.01.037
66. Yuan M, Huang D, Lee CCD, et al. Structural and functional ramifications of antigenic drift in recent SARS-CoV-2 variants. *Science*. 2021;373:818-823. doi:10.1126/science.abh1139
67. Sridhar S, Saha G, Lata S, Mehrotra R. Molecular docking studies of Indian variants of pathophysiological proteins of SARS-CoV-2 with selected drug candidates. *J Genet*. 2021;100:64.
68. Trucchi E, Gratton P, Mafessoni F, et al. Unveiling diffusion pattern and structural impact of the most invasive SARS-CoV-2 spike mutation. BioRxiv 2020.
69. Baker NA, Sept D, Joseph S, Holst MJ, McCammon JA. Electrostatics of nanosystems: application to microtubules and the ribosome. *Proc Natl Acad Sci U S A*. 2001;98:10037-10041. doi:10.1073/pnas.181342398
70. Cutler RL, Davies AM, Creighton S, et al. Role of arginine-38 in regulation of the cytochrome c oxidation-reduction equilibrium. *Biochemistry*. 1989;28:3188-3197. doi:10.1021/bi00434a012
71. Cao Y, Wang J, Jian F, et al. Omicron escapes the majority of existing SARS-CoV-2 neutralizing antibodies. *Nature*. 2022;602:657-663. doi:10.1038/s41586-021-04385-3
72. Ou J, Lan W, Wu X, et al. Tracking SARS-CoV-2 omicron diverse spike gene mutations identifies multiple inter-variant recombination events. *Signal Transduct Target Ther*. 2022;7:138. doi:10.1038/s41392-022-00992-2
73. Chakraborty C, Saha A, Bhattacharya M, Dhama K, Agoramoorthy G. Natural selection of the D614G mutation in SARS-CoV-2 omicron (B.1.1.529) variant and its subvariants. *Mol Ther Nucleic Acids*. 2023;31:437-439. doi:10.1016/j.omtn.2023.01.013
74. Kumar S, Karuppanan K, Subramaniam G. Omicron (BA.1) and sub-variants (BA.1.1, BA.2, and BA.3) of SARS-CoV-2 spike infectivity and pathogenicity: a comparative sequence and structural-based computational assessment. *J Med Virol*. 2022;94:4780-4791. doi:10.1002/jmv.27927
75. Mahase E. Covid-19: what do we know about omicron sublineages? *BMJ*. 2022;376:o358. doi:10.1136/bmj.o358
76. Liu L, Iketani S, Guo Y, et al. Striking antibody evasion manifested by the omicron variant of SARS-CoV-2. *Nature*. 2021;602:676-681. doi:10.1038/s41586-021-04388-0
77. An K, Zhu X, Yan J, Xu P, Hu L, Bai C. A systematic study on the binding affinity of SARS-CoV-2 spike protein to antibodies. *AIMS Microbiol*. 2022;8:595-611. doi:10.3934/microbiol.2022038
78. Han P, Li L, Liu S, et al. Receptor binding and complex structures of human ACE2 to spike RBD from omicron and delta SARS-CoV-2. *Cell*. 2022;185:630-640.e10. doi:10.1016/j.cell.2022.01.001
79. Khan A, Waris H, Rafique M, et al. The omicron (B.1.1.529) variant of SARS-CoV-2 binds to the hACE2 receptor more strongly and escapes the antibody response: insights from structural and simulation data. *Int J Biol Macromol*. 2022;200:438-448. doi:10.1016/j.ijbiomac.2022.01.059
80. Forssen P, Samuelsson J, Lacki K, Fornstedt T. Advanced analysis of biosensor data for SARS-CoV-2 RBD and ACE2 interactions. *Anal Chem*. 2020;92:11520-11524. doi:10.1021/acs.analchem.0c02475
81. Buratto D, Saxena A, Ji Q, Yang G, Pantano S, Zonta F. Rapid assessment of binding affinity of SARS-COV-2 spike protein to the human angiotensin-converting enzyme 2 receptor and to neutralizing biomolecules based on computer simulations. *Front Immunol*. 2021;12:730099. doi:10.3389/fimmu.2021.730099
82. Huang Y, Harris BS, Minami SA, et al. SARS-CoV-2 spike binding to ACE2 is stronger and longer ranged due to glycan interaction. *Biophys J*. 2022;121:79-90. doi:10.1016/j.bpj.2021.12.002
83. Ellis D, Brunette N, Crawford KHD, et al. Stabilization of the SARS-CoV-2 spike receptor-binding domain using deep mutational scanning and structure-based design. *Front Immunol*. 2021;12:710263. doi:10.3389/fimmu.2021.710263
84. Kang YF, Sun C, Zhuang Z, et al. Rapid development of SARS-CoV-2 spike protein receptor-binding domain self-assembled nanoparticle vaccine candidates. *ACS Nano*. 2021;15:2738-2752. doi:10.1021/acsnano.0c08379
85. Malladi SK, Singh R, Pandey S, et al. Design of a highly thermotolerant, immunogenic SARS-CoV-2 spike fragment. *J Biol Chem*. 2021;296:100025. doi:10.1074/jbc.RA120.016284
86. Millet JK, Whittaker GR. Physiological and molecular triggers for SARS-CoV membrane fusion and entry into host cells. *Virology*. 2018;517:3-8. doi:10.1016/j.virol.2017.12.015
87. Fraser BJ, Beldar S, Seitova A, et al. Structure and activity of human TMPRSS2 protease implicated in SARS-CoV-2 activation. *Nat Chem Biol*. 2022;18:963-971. doi:10.1038/s41589-022-01059-7
88. Xu C, Wang Y, Liu C, et al. Conformational dynamics of SARS-CoV-2 trimeric spike glycoprotein in complex with receptor ACE2 revealed by cryo-EM. *Sci Adv*. 2021;7:eabe5575. doi:10.1126/sciadv.abe5575
89. Willett BJ, Grove J, MacLean OA, et al. The hyper-transmissible SARS-CoV-2 omicron variant exhibits significant antigenic change, vaccine escape and a switch in cell entry mechanism. MedRxiv 2022.
90. Peacock TP, Brown JC, Zhou J, et al. The SARS-CoV-2 variant, omicron, shows rapid replication in human primary nasal epithelial cultures and efficiently uses the endosomal route of entry. *BioRxiv*, 2021.2012. 2031.474653 2022.
91. Sungnak W, Huang N, Bécavin C, et al. SARS-CoV-2 entry factors are highly expressed in nasal epithelial cells together with innate immune genes. *Nat Med*. 2020;26:681-687. doi:10.1038/s41591-020-0868-6
92. Rossi AD, de Araújo JLF, de Almeida TB, et al. Association between ACE2 and TMPRSS2 nasopharyngeal expression and COVID-19 respiratory distress. *Sci Rep*. 2021;11:9658. doi:10.1038/s41598-021-88944-8
93. Hui KPY, Ho JCW, Cheung MC, et al. SARS-CoV-2 omicron variant replication in human bronchus and lung ex vivo. *Nature*. 2022;603:715-720. doi:10.1038/s41586-022-04479-6
94. Abdelnabi R, Foo CS, Zhang X, et al. The omicron (B.1.1.529) SARS-CoV-2 variant of concern does not readily infect Syrian hamsters. *Antiviral Res*. 2022;198:105253. doi:10.1016/j.antiviral.2022.105253
95. Kwon D. Omicron's molecular structure could help explain its global takeover. *Nature*. 2022;602:373-374. doi:10.1038/d41586-022-00292-3
96. Hok L, Rimac H, Mavri J, Vianello R. COVID-19 infection and neurodegeneration: computational evidence for interactions between the SARS-CoV-2 spike protein and monoamine oxidase enzymes. *Comput Struct Biotechnol J*. 2022;20:1254-1263. doi:10.1016/j.csbj.2022.02.020
97. Watanabe Y, Allen JD, Wrapp D, McLellan JS, Crispin M. Site-specific glycan analysis of the SARS-CoV-2 spike. *Science*. 2020;369:330-333. doi:10.1126/science.abb9983
98. Abduljalil JM, Elghareib AM, Samir A, Ezat AA, Elfiky AA. How helpful were molecular dynamics simulations in shaping our

understanding of SARS-CoV-2 spike protein dynamics? *Int J Biol Macromol*. 2023;242:125153. doi:10.1016/j.ijbiomac.2023.125153

99. Maity S, Acharya A. Many roles of carbohydrates: a computational spotlight on the coronavirus S protein binding. *Acs Appl Bio Mater*. 2023. doi:10.1021/acsabm.2c01064
100. Casalino L, Gaieb Z, Goldsmith JA, et al. Beyond shielding: the roles of glycans in the SARS-CoV-2 spike protein. *ACS Cent Sci*. 2020;6:1722-1734. doi:10.1021/acscentsci.0c01056
101. Zhao P, Praissman JL, Grant OC, et al. Virus-receptor interactions of glycosylated SARS-CoV-2 spike and human ACE2 receptor. *Cell Host Microbe*. 2020;28:586-601.e586. doi:10.1016/j.chom.2020.08.004
102. Capraz T, Kienzl NF, Laurent E, et al. Structure-guided glyco-engineering of ACE2 for improved potency as soluble SARS-CoV-2 decoy receptor. *Elife*. 2021;10:e73641. doi:10.7554/eLife.73641
103. Acharya A, Lynch DL, Pavlova A, Pang YT, Gumbart JC. ACE2 glycans preferentially interact with SARS-CoV-2 over SARS-CoV. *Chem Commun (Camb)*. 2021;57:5949-5952. doi:10.1039/d1cc02305e
104. Mehdipour AR, Hummer G. Dual nature of human ACE2 glycosylation in binding to SARS-CoV-2 spike. *Proc Natl Acad Sci U S A*. 2021;118:e2100425118. doi:10.1073/pnas.2100425118
105. Pang YT, Acharya A, Lynch DL, Pavlova A, Gumbart JC. SARS-CoV-2 spike opening dynamics and energetics reveal the individual roles of glycans and their collective impact. *Commun Biol*. 2022;5:1170. doi:10.1038/s42003-022-04138-6
106. Burnap SA, Struwe WB. Mass photometry reveals SARS-CoV-2 spike stabilisation to impede ACE2 binding through altered conformational dynamics. *Chem Commun (Camb)*. 2022;58:12939-12942. doi:10.1039/d2cc04711j
107. Sali A, Blundell TL. Comparative protein modelling by satisfaction of spatial restraints. *J Mol Biol*. 1993;234:779-815. doi:10.1006/jmbi.1993.1626
108. Lee FS, Chu ZT, Warshel A. Microscopic and semimicroscopic calculations of electrostatic energies in proteins by the POLARIS and ENZYMIX programs. *J Comput Chem*. 1993;14:161-185.
109. Kamerlin SC, Vicatos S, Dryga A, Warshel A. Coarse-grained (multiscale) simulations in studies of biophysical and chemical systems. *Annu Rev Phys Chem*. 2011;62:41-64. doi:10.1146/annurev-physchem-032210-103335
110. Warshel A, Sharma PK, Kato M, Parson WW. Modeling electrostatic effects in proteins. *Biochim Biophys Acta*. 2006;1764:1647-1676. doi:10.1016/j.bbapap.2006.08.007
111. Warshel A, Russell ST. Calculations of electrostatic interactions in biological systems and in solutions. *Q Rev Biophys*. 1984;17:283-422. doi:10.1017/s0033583500005333
112. Vicatos S, Roca M, Warshel A. Effective approach for calculations of absolute stability of proteins using focused dielectric constants. *Proteins*. 2009;77:670-684. doi:10.1002/prot.22481

SUPPORTING INFORMATION

Additional supporting information can be found online in the Supporting Information section at the end of this article.

How to cite this article: An K, Yang X, Luo M, et al. Mechanistic study of the transmission pattern of the SARS-CoV-2 omicron variant. *Proteins*. 2024;1-15. doi:10.1002/prot.26663